Inhibitory of Newly Synthesized 3-BrPhOXTs on Corrosion of Stainless Steel in Acidic Medium

Ali Ehsani[a,*], Reza Moshrefi[b], Ahmad Khodadadi[c] and Ali Yeganeh-Faal[c]

[a]*Department of Chemistry, Faculty of Science, University of Qom, Qom, Iran.*
[b]*Department of Chemistry, Faculty of Science, K.N. Toosi University of Technology, Tehran, Iran.*
[c]*Department of Chemistry, Faculty of Sciences, Payame Noor University, Iran.*

ABSTRACT

Newly synthesized 3-(3-bromophenyl)-2-imino-2,3-dihydrobenzo[*d*]oxazol-5-yl 4-methylbenzenesulfonate (3-BrPhOXTs) inhibitoRY effect on the corrosion of stainless steel L316 (SS) in sulfuric acid was investigated by means of potentiodynamic polarization and electrochemical impedance spectroscopy (EIS). According to electrochemical results, excellent inhibiting properties for SS corrosion in sulfuric acid has been obtained. The adsorption of 3-BrPhOXTs onto the SS surface followed the Langmuir adsorption model with the free energy of adsorption ΔG^0_{ads} of –8.94 kj mol^{-1}.

KEYWORDS

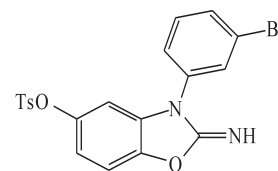Organic inhibitor, adsorption, stainless steel, impedance.

1. Introduction

Type 316L stainless steel has received considerable attention in the corrosion community, due to extensive application in environments where pitting resistance is required. It is well known to retard rate of metal dissolution in acid such as hydrochloric acid solutions that are widely use for cleaning, pickling, descaling and etching of steel. The use of an additive is one of the major solutions of this problem. Hence, various additives are used to protect iron and its alloys against corrosive attack.[1–5] The use of an inhibitor is one of the best known methods for corrosion protection from corrosive acid media. Heterocyclic compounds containing multiple heteroatoms such as O, N, and S act as effective inhibitors for the corrosion of steel in pickling acid media and have been the subject of many publications.[6–10] The compounds containing both nitrogen and sulfur in their molecular structure have exhibited greater inhibition compared with those possessing only one of these atoms.[11–13] In the literature, many thiazole derivatives have been reported as corrosion inhibitors and found to have good corrosion inhibition effect.[14,15] The efficiency of an organic compound inhibitor is mainly dependent on its ability to adsorb on a metal surface, which consists of replacement of a water molecule at a corroding interface. In this study electrochemical tests were employed to investigate the inhibition performance of newly synthesized 3-BrPhOXTs in acidic solution.

2. Experimental

2.1. Material

Stainless steel 316L has the composition (wt %) Fe: 67.95, Ni: 10.60, Si: 0.45, Mn: 1.75, Cr: 16.50, S: 0.025, P: 0.028, Mo: 2.10, Al: 0.008, Co: 0.16, Cu: 0.35, Nb: 0.01 and V: 0.02. The SS surface was ground with silicon carbide abrasive paper from 400 to 1200, degreased with absolute ethanol, rinsed in distilled water, and dried in warm air. The corrosive medium was 0.5 M H_2SO_4 solution prepared from analytical reagent grade 98 % sulfuric acid and distilled water. 3-(3-bromophenyl)-2-imino-2,3-dihydrobenzo[*d*]oxazol-5-yl 4-methylbenzenesulfonate

* To whom correspondence should be addressed. E-mail: ehsani46847@yahoo.com / a.ehsani@qom.ac.ir

Scheme 1
Structure of 3-(3-bromophenyl)-2-imino-2,3-dihydro-benzo[*d*]oxazol-5-yl 4-methylbenzenesulfonate.

(Scheme 1) was synthesized in our laboratory from the reaction between 3-(3-bromophenyl)-2-imino-2,3-dihydrobenzo[*d*]oxazol-5-ol with *p*-toluene sulfonyl chloride and K_2CO_3 in EtOH under ultrasound irradiation for 1.5 h at room temperature.[16–22] The crude product was purified by recrystalization in aqueous ethanol to afford the pure product (Yield 87 %) and characterized by ^{1}H NMR, ^{13}C NMR, FT-IR, elemental analysis (CHN), and melting points. M.p. 189–190 °C; FT-IR (KBr, cm^{-1}): 3334, 3086, 1702, 1590, 1495, 1478, 1430, 1388, 1363, 1221, 1192, 1171, 1135, 1092, 1071, 996, 888, 868, 850, 818, 784, 742, 722, 700, 684, 665, 653, 617, 594, 554, 520; ^{1}H NMR (400 MHz, DMSO-d_6): δ_H = 7.72 (d, *J* = 8.4 Hz, 2H), 7.64–7.61 (m, 2H), 7.45–7.44 (m, 2H), 7.37 (d, *J* = 8.4 Hz, 3H), 7.09 (d, *J* = 8.8 Hz, 1H), 6.69 (d, *J* = 8.8 Hz, 1H), 6.59 (d, *J* = 2.4 Hz, 1H), 2.49 (s, 3H); ^{13}C NMR (100 MHz, DMSO-d_6): δ_C = 156.2, 145.7, 145.6, 142.9, 135.3, 133.2, 131.9, 131.6, 131.3, 129.9, 128.7, 128.6, 124.2, 123.3, 116.1, 109.4, 103.5, 21.8; CHN: Anal. Calcd for $C_{20}H_{15}BrN_2O_4S$: C, 52.30; H, 3.29; N, 6.10. Found: C, 52.42; H, 3.37; N, 6.21. ^{1}H NMR, ^{13}C NMR and FT-IR spectra are presented in the online supplement.

The concentration range of (3-BrPhOXTs) employed was 1×10^{-4} to 10^{-3} M in 0.5 M sulfuric acid.

2.2. Equipment

All electrochemical measurements were carried out in a conventional three-electrode cell, powered by a potentiostat/galvanostat (EG&G 273A) and a frequency response analyzer (EG&G, 1025). The system was operated from a PC utilizing M270 and M398 software *via* a GPIB interface. The frequency range of 100 kHz to 15 mHz and modulation amplitude of 5 mV were employed for impedance studies. A SS electrode was

employed as the working electrode. A saturated calomel electrode (SCE) and a platinum wire were used as reference and counter electrodes, respectively. Before measurement, the working electrode was immersed in test solution for approximately 1 h until a steady open circuit potential (OCP) was reached. The polarization curves were carried out from cathodic potential of –1.4 V to anodic potential of 0.10 V with respect to the open circuit potential at a sweep rate of 0.5 mV s⁻¹. The linear Tafel segments of the anodic and cathodic curves were extrapolated to corrosion potential (E_{corr}) to obtain the corrosion current densities (i_{corr}). In each measurement, a fresh working electrode was used. Several runs were performed for each measurement to obtain reproducible data.

3. Results and Discussion

3.1. Potentiodynamic Polarization Studies

Potentiodynamic polarization experiments were carried out to ascertain the influence of inhibitor on the kinetics of the anodic and cathodic partial reactions of the corrosion process. Figure 1 depicts typical potentiodynamic polarization curves for the SS specimen in 0.5 M H_2SO_4 and without and with different concentration of inhibitor. The corresponding polarization parameters are presented in Table 1. In corrosion, quantitative
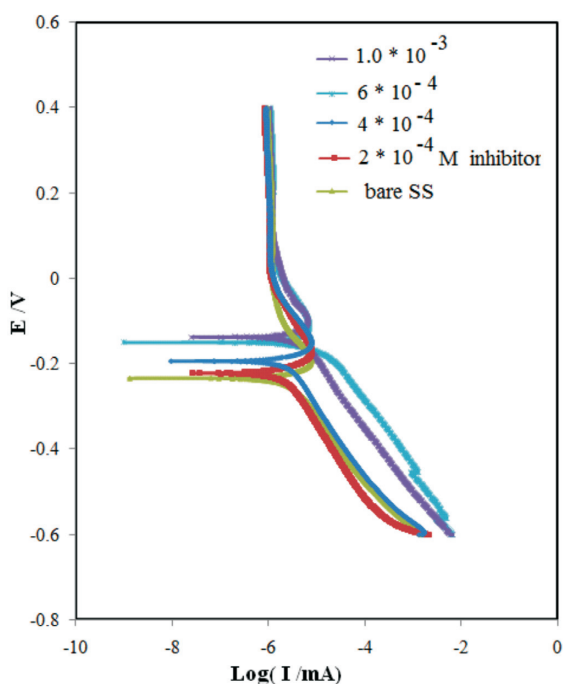
information on corrosion currents and corrosion potentials can be extracted from the slope of the curves, using the Stern-Geary equation, as follows:[23,24]

$$i_{corr} = \frac{1}{2.303 R_p}\left(\frac{\beta_\alpha \times \beta_c}{\beta_a + \beta_c}\right) \tag{1}$$

i_{corr} is the corrosion current density in amps cm⁻²; R_p is the corrosion resistance in ohms cm²; β_a is the anodic Tafel slope in volts/decade or mV/decade of current density; β_c is the cathodic Tafel slope in volts/decade or mV/decade of current density; the quantity, $\left(\frac{\beta_\alpha \times \beta_c}{\beta_a + \beta_c}\right)$, is referred to as the Tafel constant. The corrosion inhibition efficiency was calculated using the relation:[24]

$$\eta\,(\%) = 100\left(\frac{i_{corr}^* - i_{corr}}{i_{corr}^*}\right) \tag{2}$$

where i^*_{corr} and i_{corr} are uninhibited and inhibited corrosion current densities, respectively, determined by extrapolation of Tafel lines in the corrosion potential. The corrosion rates v (mm year⁻¹) from polarization were calculated using the following equation:[24]

$$v = \frac{i_{corr} \times t \times M}{F \times S \times d} \times 10 \tag{3}$$

where t is the time (s), M is the equivalent molar weight of working electrode (g mol⁻¹), F is Faraday constant (96500 C mol⁻¹), S is the surface area of electrode, d is the density of iron and the constant 10 is used to convert the unit cm to mm. The results are presented in Table 1. The inhibitor molecule first adsorbs on the SS surface and blocks the available reaction sites. As the concentration of the inhibitor increases, the linear polarization resistance increases and the corrosion rate decreases. The surface coverage increases with the 3-BrPhOXTs concentration and the formation of 3-BrPhOXTs film on the SS surface reduces the active surface area available for the attack of the corrosive solution and delays hydrogen evolution reaction (HER) as a cathodic reaction and SS dissolution.[24] In the cathodic branch, as seen in Table 1, the values of β_c reveal small changes with increasing 3-BrPhOXTs concentration, which indicates that the 3-BrPhOXTs is adsorbed on the SS surface and the addition of the 3-BrPhOXTs hinders the acid attack on the SS electrode. In anodic branch, the value of β_a decreases with the presence of 3-BrPhOXTs. The shift in the anodic Tafel slope (β_a) might be related to the modification of anodic dissolution process due to the inhibitor modules adsorption on the active sites of the SS. Compared to the absence of 3-BrPhOXTs, the anodic curves of the working electrode in the acidic solution containing the 3-BrPhOXTs clearly shifted to the direction of current reduction, as it could be observed from these polarization results; the inhibition efficiency increased with inhibitor concentration reaching a maximum value of 80.68 % at 10⁻³ mol L⁻¹.

Figure 1 Potentiodynamic polarization curves of SS in 0.5 M H_2SO_4 solution in the absence and presence of various concentrations of the 3-BrPhOXTs.

Table 1 Corrosion parameters obtained from Tafel polarization curves of SS 316L in 0.5 M H_2SO_4 in the absence and presence of different concentrations of 3-BrPhOXTs at 298 K.

Inhib. Conc.	β_a*/V/decade	β_c* V/decade	I/uA	E/v	CR/mpy
0	0.61	0.14	12.76	–0.22	5.25
0.0002M	0.63	0.18	11.93	–0.15	4.61
0.0004M	0.07	0.18	5.43	–0.14	2.23
0.0006M	0.07	0.17	3.26	–0.23	1.34
0.0008M	0.06	0.18	2.49	–0.22	1.024
0.001M	0.03	0.17	2.46	–0.19	1.014

* β_a is anodic Tafel slope and β_c is cathodic Tafel slope.

3.2. Electrochemical Impedance Spectroscopy (EIS)

Electrochemical impedance spectroscopy is one of the powerful techniques for analyzing the characteristics of the conducting polymer modified electrodes and charge transfer mechanism in the electrolyte/electrode interface. This has been broadly discussed in the literature using a variety of theoretical models.[23–32] Impedance measurements were performed under potentiostatic conditions after 1 h of immersion. Nyquist plots of solutions containing different concentrations of 3-BrPhOXTs molecules were performed over the frequency range from 100 kHz to 100 mHz and are shown in Fig. 2. The similarity in the shapes of these plots throughout the experiment shows that the addition of 3-BrPhOXTs molecules does not cause any significantly changes in the corrosion mechanism. The Nyquist plots show one capacitive semicircle at high frequencies. The capacitive semicircles at high frequencies shows the process associated with the electrical double layer in the SS and electrolyte interface. Nyquist plot contain depressed semicircles with the centre under the real axis. Such depressed semicircle is characteristic of solid electrodes and often referred to as frequency dispersion, attributed to different physical process such as roughness, fractality nature of the solid surfaces, impurities, grain boundaries, and distribution of surface active sites. The ideal capacitive behaviour is not observed in this case and hence a constant phase element (CPE) is introduced in the circuit to give a more accurate fit.[27–34] The simplest fitting is represented by Randle's equivalent circuit[34] (Fig. 2), which is a parallel combination of the charge transfer resistance (R_{ct}) and CPE, both in series with the solution and electrode resistance (R_s).

The following equation used for calculating the percentage inhibition efficiency:[34]

$$\eta(\%) = 100\left(\frac{R_{ct}^* - R_{ct}}{R_{ct}^*}\right) \tag{4}$$

where R_{ct}^* and R_{ct} are values of the charge transfer resistance observed in the presence and absence of inhibitor. Impedance parameters are summarized in Table 2. The results obtained from polarization and electrochemical impedance spectroscopy techniques shows reasonable change and are nearly close. As observed in Table 2, the adsorption of 3-BrPhOXTs molecules on SS surface alters the interface between the corrosive solution and metal surface and decreases its electrical capacity. The increase in R_{ct} values with increase in 3-BrPhOXTs concentration can be interpreted as the formation of an insulated adsorption layer. At the highest inhibitor concentration of 10^{-3} mol L^{-1}, the inhibition efficiency significantly increases and reaches 81.17 %. Thus, it can be deduced that 3-BrPhOXTs has a major role in SS protection at the concentration of 10^{-3} M.

3.3. Adsorption Isotherms

The adsorption of an organic molecule at metal/solution interface can be demonstrated as a substitution adsorption process between the organic molecules in aqueous solution, (Org$_{aq}$), and the water molecules on SS surface, (H$_2$O$_{ads}$)Org$_{aq}$:[34]
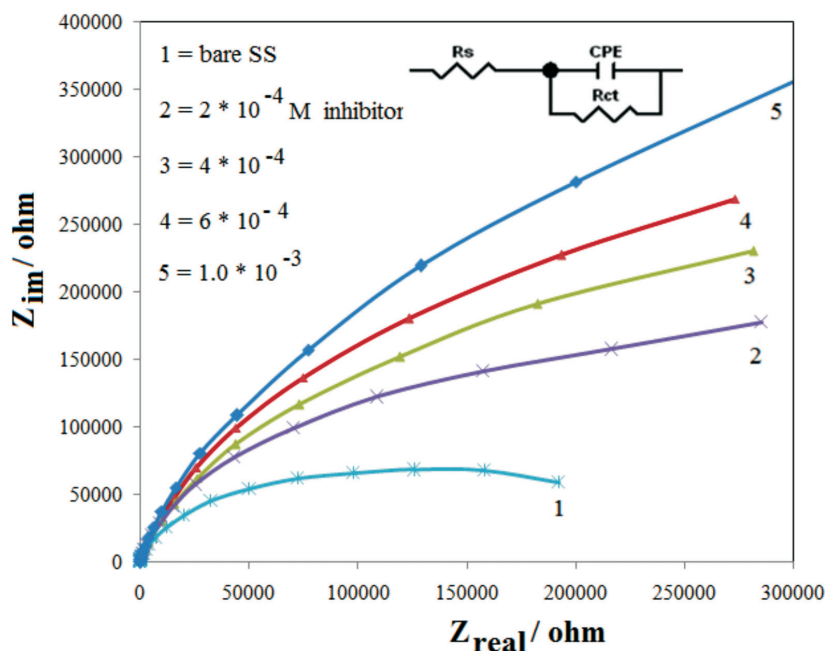

Figure 2 Nyquist plots of SS in 0.5 M H$_2$SO$_4$ solution containing different concentrations of the 3-BrPhOXTs. Electrical equivalent circuit used for modeling metal/solution interface in the absence and presence of inhibitors. Data for the Nyquist plots are presented in the online supplement.

Table 2 Impedance parameters for the corrosion of SS in 0.5M H$_2$SO$_4$ containing different concentration of 3-BrPhOXTs at 298 K.

Concentration/M	R_s/Ω	$Y_0^*/\mu\Omega^{-1}\,s^n$	n^*	R_{ct}/Ω	IE%
0	4.25	152.85	0.89	12.35	
2.0×10^{-4}	4.89	131.22	0.85	21.12	41.52
4.0×10^{-4}	5.79	95.51	0.84	32.44	61.92
6.0×10^{-4}	7.24	74.86	0.81	45.36	72.27
8.0×10^{-4}	8.16	68.32	0. 79	58.17	78.76
1.0×10^{-3}	8.84	63.46	0.78	65.61	81.17

*Y_0 and n are non-ideal capacitor elements in the case of CPE.
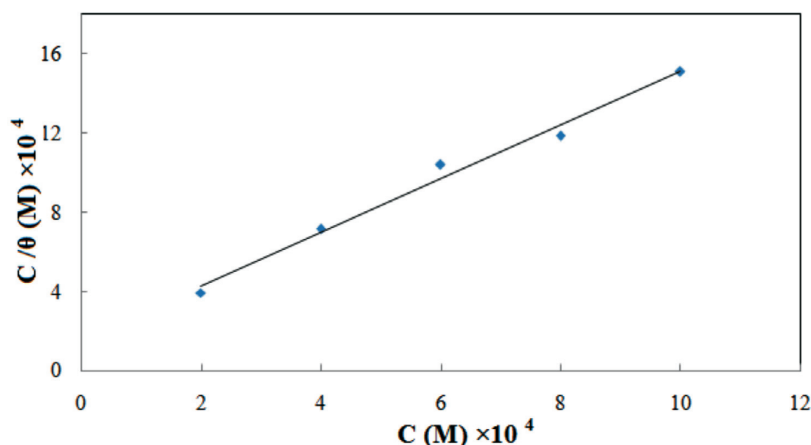
Figure 3 Langmuir adsorption plot for SS in 0.5 M H_2SO_4 containing different concentrations of 3-BrPhOXTs.

$$Org_{aq} + XH_2O_{ads} \leftrightarrow Org_{ads} + XH_2O_{aq} \qquad (5)$$
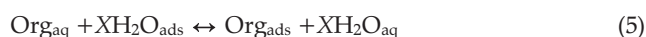
where X, the size ratio, is the number of water molecules displaced by one molecule of organic molecule. X is assumed to be independent of coverage or charge on the electrode.[32] Basic information on the interaction between the organic molecules and the SS surface is provided by the adsorption isotherm. The degree of surface coverage, θ, at different concentrations of organic compounds in 0.5 M H_2SO_4 was evaluated from polarization measurements (θ = IE(%)/100) at 25 °C. The plot of C/θ against inhibitor concentration, C, displayed a straight line for the tested inhibitor (Fig. 3). The linear plot clearly showed that the surface adsorption process of 3-BrPhOXTson the SSsurface follows the Langmuir isotherm. Likewise, it suggests that an adsorption process occurs, which can be expressed as follows:[34]

$$\frac{C}{\theta} = \frac{1}{K_{ads}} + C \qquad (6)$$

where K_{ads} is the equilibrium constant of the adsorption process. Free energy of adsorption (ΔG_{ads}) can be obtained by Eq. (7). The numeral of 55.5 is the molar concentration of water in the solution:[34]

$$K_{ads} = \frac{1}{55.5} \exp\left(\frac{-\Delta G^0_{ads}}{RT}\right) \qquad (7)$$

The value of ΔG^0 ads for adsorption of 3-BrPhOXTs was obtained to be 8.94 kJ mol^{-1}. The negative value of ΔG^0 suggests that 3-BrPhOXTs is spontaneously adsorbed on the SS surface.[34–38] The adsorption of an organic compound on the SS can occur on the basis of donor–acceptor interactions between the p-electrons of the organic compound and the vacant d-orbitals of the SS surface atoms.

4. Conclusion

From the results, it is obvious that 3-BrPhOXTsacts as a good inhibitor for corrosion of SS in the 0.5 M H_2SO_4 solution. From the electrochemical studies, it is evident that 3-BrPhOXTs acts as a mixed type inhibitor in 0.5 M H_2SO_4solution. EIS plots indicate that the charge transfer resistances increase with increasing concentration of the inhibitor at the highest inhibitor concentration of 10^{-3} mol L^{-1}, the inhibition efficiency increases. 3-BrPhOXTs inhibits corrosion by getting adsorbed on the metal surface following Langmuir adsorption isotherm.

Supplementary data

Supplementary data are presented in the online supplement.

References

1 I. Ahamad and M.A. Quraishi, *Corros. Sci.*, 2009, **51**, 2006–2013.

2 Q.B. Zhang and Y.X. Hua, *Electrochim. Acta*, 2009, **54**, 1881–1887.

3 W. Li, Q. He, C. Pei and B. Hou, *Electrochim. Acta*, 2007, **52**, 6386–6394.

4 R. Solmaz, G. Kardas, B. Yazıcı and M. Erbil, *Prot. Met.*, 2005, **41**, 581–585.

5 G. Kardas, *Mater. Sci*, 2005, **41**, 337–343.

6 J. Aljourani, K. Raeissi and M.A. Golozar, *Corros. Sci.*, 2009, **51**, 1836–1843.

7 M.L. Zheludkevich, K.A. Yasakau, S.K. Poznyak and M.G.S. Ferreira, *Corros. Sci.*, 2005, **47**, 3368–3383.

8 I.B. Obot, N.O. Obi-Egbedi and S.A. Umoren, *Corros. Sci.*, 2009, **51**, 276–282.

9 M.G. Hosseini, M. Ehteshamzadeh and T. Shahrabi, *Electrochim. Acta*, 2007, **52**, 3680–3685.

10 S. Afak, B, Duran, A. Yurt and G. Turkoglu, *Corros. Sci.*, 2012, **54**, 251–259.

11 H.H. Hassan, E. Adbelghani and M.A. Amin, *Electrochim. Acta*, 2007, **52**, 6359–6366.

12 Y. Abdoud, A. Abourrriche, T. Saffaj, M. Berrada, M. Charrouf, A. Bennamara, N. Al Himidi and H. Hannache, *Mater. Chem. Phys.*, 2007, **105**, 1–5.

13 M.A. Quaraishi, J. Rawat and M. Ajmal, *J. Appl. Electrochem.*, 2000, **30**, 745–751.

14 K.F. Khaled and M.A. Amin, *Corros. Sci.*, 2009, **51**, 1964–1975.

15 I.B. Obot and N.O. Obi-Egbedi, *Corros. Sci.*, 2010, **52**, 282–285.

16 D. Habibi, M. Nasrollahzadeh, H. Sahebekhtiari andR.V. Parish, *Tetrahedron* 2013, **69**, 3082–3087.

17 A.R. Modarresi-Alam and M. Nasrollahzadeh, *Turk. J. Chem.*, 2009, **33**, 267–280.

18 D. Habibi, M. Nasrollahzadeh, L. Mehrabi and S. Mostafaee, *Monatsh. Chem.*, 2013, **144**, 725–728.

19 D. Habibi, M. Nasrollahzadeh and Y. Bayat. *Synth. Commun.*, 2011, **41**, 2304.

20 D. Habibi and M. Nasrollahzadeh. *Synth. Commun.*, 2012, **42**, 2023–2032.

21 D. Habibi, M. Nasrollahzadeh, A.R. Faraji and Y. Bayat, *Tetrahedron*, 2010, **66**, 3866–3870.

22 M. Nasrollahzadeh, D. Habibi, Z. Shahkarami and Y. Bayat, *Tetrahedron*, 2009, **65**, 10715–10719.

23 M.G. Mahjani, R. Moshrefi, A. Ehsani and M. Jafarian, *Anti-Corros. Methods Mater.*, 2011, **58**, 250–257.

24 T. Zhihua, Z. Shengtao, L. Weihua and H. Baorong, *Ind. Eng. Chem. Res.*, 2011, **50**, 6082–6088.

25 A. Ehsani, M.G. Mahjani and M. Jafarian, *Turk. J. Chem.*, 2011, **35**, 1–9.

26 A. Ehsani, M.G. Mahjani and M. Jafarian, A. Naeemy, *Electrochim. Acta*, 2012, **71**, 128–133.

27 A. Ehsani, B. Jaleh and M. Nasrollahzadeh, *J. Power Sources*, 2014, **257**, 300–307.

28 A. Ehsani, M.G. Mahjani, S. Adeli and S. Moradkhani, *Prog. Org. Coat.*, 2014, **77**, 1674–1681.

29 A. Ehsani, M.G. Mahjani, M. Bordbar and S. Adeli, *J. Electroanal. Chem.*, 2013, **710**, 29–35.

30 A. Ehsani, F. Babaei and M. Nasrollahzadeh, *Appl. Surf. Sci.*, 2013, **283**, 1060–1064.

31 A. Ehsani, S. Adeli, F. Babaei, H. Mostaanzadeh and M. Nasrollahzadeh, *J. Electroanal. Chem.*, 2014, **713**, 91–97.

32 A. Ehsani, M.G. Mahjani, M. Jafarian and A. Naeemy, *Prog. Org. Coat.*, 2010, **69**, 510–516.

33 A. Ehsani, M.G. Mahjani and M. Jafarian, *Synth. Meth.*, 2011, **161**, 1760–1765.

34 A. Ehsani, M. Nasrollahzadeh, MG. Mahjani, R. Moshrefi and H. Mostaanzadeh, *J. Indus. Eng. Chem.*, 2014, **20**, 4363–4370.

35 A. Ehsani, M.G. Mahjani, R. Moshrefi, H. Mostaanzadeh and J. Shabani-Shayeh, *RSC Adv.,* 2014, **4**(38), 20031–20037.

36 H. Hassan, *Electrochim. Acta,* 2006, **51**, 5966-5972.

37 S. Martinez, *Mater. Chem. Phys.*, 2002, **77**, 97–102.

38 I.B. Obot, N.O. Obi-Egbedi and S.A. Umoren, *Corros. Sci.*, 2009, **51**, 1869.